LA-UR-01-1534

Radiofrequency remote sensing of lightning from space: a study of thunderstorm detectability and lightning discrimination using the FORTE satellite, groundtruthed by NLDN

Abram R. Jacobson (corresponding author), Tracy E. Light, and
David M. Suszcynsky
Space and Atmospheric Sciences Group
Mail Stop D466
Los Alamos National Laboratory
Los Alamos, NM 87545

Rough draft: 12 March 2001
To be submitted to Journal of Geophysical Research

Abstract

Radio signals high enough in frequency (>25 MHz) to reliably penetrate the ionosphere provide a means (complementary to optical) for satellite-based remote sensing of lightning. Seen from space, lighting radiofrequency signals must be exceptionally intense to compete with anthropogenic radio noise. This leads to the RF lightning observables seen from space being rather atypical of the electromagnetic signatures of lightning described in the literature on ground-based observations. We have used a two-year campaign of joint observations over the North America region to better understand the how FORTE "sees" storms (via their radiofrequency observables) that are also "seen" and characterized by the National Lightning Detection Network via their direct low-frequency (<100 kHz) radiation. We find that FORTE's radiofrequency events are likely to be associated with the same storms as detected by NLDN, but that beyond that, the information provided by space-based RF detection is dominated by intracloud processes, regardless of NLDN's dominant stroke type for the storm. Even in the case of close temporal coincidence between FORTE RF events and NLDN ground-return strokes, the RF emission tends to occur high in the cloud. There is an important exception to this rule, which is a spectacularly narrow and coherent RF emission during negative cloud-to-ground strokes over seawater.

(1) Introduction

Radiofrequency (RF) emissions from lightning processes offer a means of remotely sensing lightning from space [*Holden et al.*, 1995; *Jacobson et al.*, 2000; *Jacobson et al.*, 1999; *Massey and Holden*, 1995; *Massey et al.*, 1998a]. This remote-sensing capability in turn might eventually allow a constellation of radio-frequency receivers on satellites to perform real-time tracking of the deep tropospheric convection with which lightning is

associated in at least some well-characterized and important weather regimes [*Boccippio et al.*, 2000; *Petersen and Rutledge*, 1998; *Zipser*, 1994; *Zipser and Lutz*, 1994]. At present we do not know how to infer detailed convective-storm characteristics from RF signals collected in space. However, it is already clear that the very appearance of active radiofrequency emissions high in the troposphere is an early sign of developing deep convection.

If there is developed a practical RF convection monitoring capability that is truly global, it will likely have to "piggy-back" on existing spaceborne assets [*Suszcynsky et al.*, 2000a]. The observation of lightning from space offers the opportunity to view the whole Earth synoptically. However, the view of the Earth from orbit is very RF-noisy due to anthropogenic continuous-wave and modulated RF communications carriers and radars [*Jacobson et al.*, 1999]. Only certain selected RF signals from lightning are detectable above the high noise background.

The principal ground-based systems for electromagnetic monitoring of lightning activity are arrays of low-frequency (LF) and very-low-frequency (VLF) sensors that provide differential-time-of-arrival geolocation of the lightning strokes responsible for the detected LF/VLF signal. The most established such system is the National Lightning Detection Network (NLDN) in the United States [*Cummins et al.*, 1998], but there are several others worldwide. The electromagnetic signals seen from such arrays in the radiation far field are horizontally-propagating (Earth-skimming, or at longer range ducted in the Earth-ionosphere waveguide) LF/VLF radiation from the vertical current component of the source strokes.

By contrast, the very-high-frequency (VHF) radiation detected by radio-frequency receivers is normally generated by the air-breakdown processes (leader growth) which either precede strokes, or which occur on their own and fail to be accompanied by detectable strokes [*Proctor*, 1981; *Proctor et al.*, 1988; *Rhodes et al.*, 1994; *Shao et al.*, 1999; *Shao and Krehbiel*, 1996; *Shao et al.*, 1995; *Taylor*, 1978; *Taylor et al.*, 1984]. Thus, the lightning signatures gathered by ground-based LF/VLF arrays on the one hand,

and by VHF receivers, on the other hand, tend to be related to complementary aspects of the complex lightning process.

From space, a VHF receiver is exposed to the cumulative radio noise, most of it anthropogenic, deriving from a large area of the Earth. For example, the FORTE satellite at altitudes near or exceeding 800 km "sees" a disk on Earth of diameter several-thousand kilometers [*Jacobson et al.*, 1999]. Except over a very few radio-quiet areas of Earth, FORTE is thus exposed to myriad communication, industrial, and radar signals within the operating passband. This tends to disfavor the reception and recognition of weak signals caused by lightning, signals that are often straightforward to receive and to recognize using a ground-based VHF system. The satellite-based receiver system is biased toward the most intense VHF emissions from lightning systems. What are these most intense VHF signals, and how are they related to the taxonomy of lightning strokes recognizable from LF/VLF observations?

(2) FORTE observations of VHF signals from lightning

The FORTE satellite has observed lightning continually since its launch on 29 August 1997. FORTE is in a 70° inclination, circular low-Earth orbit and makes several passes per day over lightning-prone tropical regions, notably South America, Africa, and SE Asia/ Indonesia, as well as over the less lightning-prone midlatitudes. FORTE captures and stores discrete records of VHF lightning signatures. The radio-frequency (rf) receiver whose data are used in this study comprises two 50-Megasample-per-second passbands, each analog-filtered to 22-MHz bandwidth. In the data to follow, we always operated the rf payload with one 22-MHz channel placed in the range 26-48 MHz, with a nominal 38-MHz center ("low band"). The performance of the FORTE rf payload, plus some of the initial characteristics of the lightning observations, have been described in detail elsewhere [*Jacobson*, 1999; *Jacobson et al.*, 1999].

There are eight “trigger subbands” in each 22-MHz-wide receiver channel. Each 1-MHz-wide trigger subband has a noise-compensation option, so that the trigger threshhold is either set in absolute level or as dB *above a low-pass-filtered noise level* in that 1-MHz subband, i.e. as a “noise-riding threshold”. In this way the trigger system can in practice trigger on lightning signatures that would otherwise be overwhelmed by anthropogenic radio carriers appearing in the overall analog passband. In the data used here, we use noise-riding-threshhold triggering and require five (out of eight) 1-MHz subbands to trigger in correlation. We typically require the signal to rise at least 14 - 20 dB (depending on the program and the intended class of lightning signals) above the noise background in each 1-MHz subband contributor to the “5-out-of-8” OR condition. These contributing channels must arrive within a coincidence time of 162 μs of each other. This coincidence window allows for arrival of different frequencies from the same event, in the presence of ionospheric dispersion of the pulse. (“Ionospheric dispersion” is the effect of the ionospheric plasma's imposing a group delay on the rf pulse, with the delay varying roughly as $1/f^2$.)

The $1/f^2$ dispersion causes the lowest frequencies to arrive latest, as in a “chirp”. For this reason the VHF signals which have been transmitted through the ionosphere are referred to as “chirped” signals. Similarly, the signal-processing step of removing the dispersion is called “de-chirping”. We perform “de-chirping” on all archived VHF signals from FORTE.

Both 22-MHz-bandwidth channels are connected to different linear polarizations of a two-polarization log-periodic antenna. The antenna is mounted on a boom toward the satellite nadir, usually within a few degrees. The antenna is designed to place an approximate minimum (throughout the VHF spectrum) on the limb of the Earth as seen from FORTE, and a lobe maximum at nadir. The limb is a circle of diameter 6,400 km on the surface of the Earth.

The Data Acquisition System (DAS) contains enough memory for up to 0.8 seconds (cumulative) of 12-bit data simultaneously from the two 22-MHz channels. Each record

is triggered (see above) and has adjustable pre/post-trigger ratio. We typically use 400-μs records with 100 μs of pretrigger samples and 300 μs of posttrigger samples. There is typically room in DAS memory for ~2000 such events between downloads. Since we can have up to several downloads per day, in principle we can acquire up to ~10000 such events per day. Usually, however, operations constraints and availability of suitable lightning storms near the FORTE track limit us to less than this theoretical maximum.

The DAS is capable of beginning a new record 162 μs after the end of the previous record, so that FORTE records can effectively mosaic-together to form a quasi-continuous registation of VHF signatures arriving one-upon-the-other within a flash. We find in practice that the registration of records is not impeded by the necessary DAS dead time between records, but rather is spaced wider apart by the natural cadence of the emission process itself.

The configuration described above was followed between launch (August 1997) and December 1999. During this ~ 28-month campaign, FORTE gathered over 3-million data records, the vast majority of which were due to VHF emissions from lightning. More recently (starting in January 2000) we have used a wider-band (85-MHz analog bandwidth), whose initial results are described elsewhere [*Light et al.*, 2001]. The 28-month campaign always had at least one receiver in the "low band", which is the Nyquist-allowed range 26-51 MHz. In practice that band is low-pass filtered to cover the range of only 26-48 MHz. All signal waveforms discussed in this paper refer to the "low band" data.

(3) FORTE/NLDN campaign statistical results

(3a) Common VHF signatures

During two six-month campaigns (April-September 1998 and May-October 1999), FORTE was tasked to gather maximum VHF data over the North American sector, and the VHF events were compared in detail to NLDN stroke-level, loosened-criterion data. The first (i.e., 1998) campaign and the systematics of the loosened criterion are described

in detail elsewhere [*Jacobson et al.*, 2000]. All results developed in this paper will be from the composite archive from both campaigns. The first campaign's statistical conclusions already described [*Jacobson et al.*, 2000] are equally descriptive of the second campaign and will not be repeated here.

A small number of FORTE VHF events are found to be closely coincident with NLDN strokes, within a range of ±300 μs after correcting for all propagation delays. During the first campaign the closely-coincident events totaled about 15-thousand. During the second campaing the total was about 10-thousand. The overall total was thus about 25-thousand closely-coincident events.

We stress that these 25-thousand events constitute a very small subset of the those FORTE events which are generated by the same storms that are detected and located by NLDN. Instead, the 25-thousand closely coincident events include only the very special subset of FORTE events which closely coincide in time with the LF/VLF emission detected by NLDN. There are many more VHF signals, coming from the same storms, which are not closely coincident with NLDN and which are therefore not amongst these 25-thousand special events, either by being elsewhere in the same flashes, or by being in entirely different flashes but within the same storm. For example, in the entire month of August 1998, FORTE collected approximately 11,000 VHF events over the CONUS, but only 30% of these were closely coincident with NLDN strokes. In August 1999, FORTE collected approximately 37,000 VHF events over the CONUS, but only 10% of these were closely coincident with NLDN strokes. (We attribute this interannual difference (1) to the lessened incidence of +CG strokes in 1999 relative to 1998, and (2) to the tendency of FORTE VHF to more likely coincide with +CG strokes declared by NLDN.)

The first example of FORTE VHF signatures is a narrow pulse that is remarkable for being poorly- and perhaps not at all -correlated in time with NLDN strokes. Figure 1 shows a typical such pulse. Each panel is a spectrogram in which the vertical axis is frequency, and the horizontal axis is time. The color scale (shown at right) encodes the square of the received electric field, in units of $(v/m)^2$. Both panels have been pre-

whitened, that is, have had their CW carriers partially suppressed [*Jacobson et al.*, 1999]. The top panel has not been "dechirped" (compensated for ionospheric dispersion), while the bottom one has. The top panel shows the entire 400-μs event, while the lower panel selects the 40 μs in which is centered the dechirped first pulse. The signal has undergone magnetic birefringent splitting into ordinary and extraordinary propagation modes [*Jacobson and Shao*, 2001; *Massey et al.*, 1998b]. The lower panel's Fourier window has an effective temporal width of approximately 0.6 μs, so the width of the features (either magnetic mode separated from the other) is not significantly above the instrumental limit. Thus, the true width of the pulse may be less than 0.6 μs.

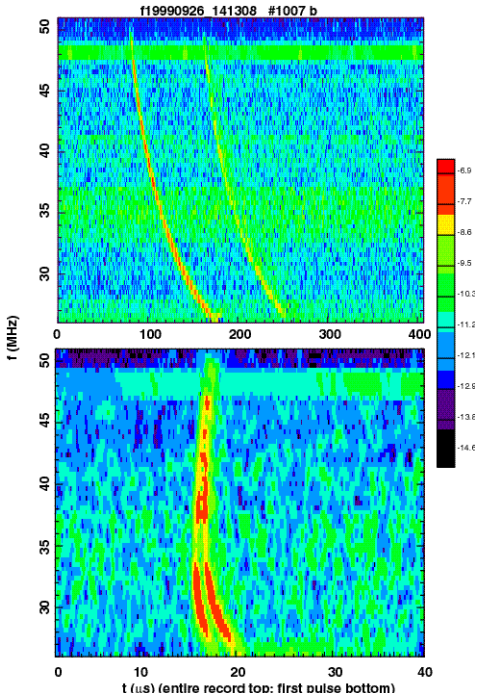

Figure 1: Spectrograms of power spectral density versus frequency (vertical axis) and time (horizontal axis) for a narrow VHF isolated pulse pair, or "VIP". The color scale is the $\log_{10}$ of square of the received electric field. The top panel shows the entire 400-μs record, while the bottom panel shows only 40 μs centered on the first pulse. The data is prewhitened in both panels but has been first-order dechirped in only the lower panel (see text). The Fourier window is 128 samples (2.56 μs) and is slid forward by 8 samples (160 ns). The weighting within the upper panel's Fourier window provides an effective time resolution of about 1.2 μs. The weighting function within the lower panel's Fourier window has less support and provides an effective time resolution of only about 600 ns.

This characteristic and important FORTE VHF pulse-pair signal exemplied by the case of Figure 1 is reliably *unassociated* with NLDN. This particular VHF signal only occasionally occurs in close coincidence with an NLDN stroke, at a rate which is less than 10% of the rate shown by ordinary (i.e., broader and totally incoherent) pulse pairs. This VHF signal exemplified in Figure 1 tends to occur in sparsely-populated (1 event per second or less frequent) random VHF-event cadences completely outside the more normal temporal clustering associated with "flashes". This VHF signal is always a pulse

pair, consisting of an initial pulse followed by its reflection from the Earth's surface. Thus it is axiomatic that this type of event occurs in the cloud or at least at cloud altitude. We shall call these "VHF isolated pulse-pairs", or VIPs for short, in what follows.

A remarkable feature of the VIP signal is its coherence, or coherence relative to the more frequent intracloud VHF pulses such as those (see below) that are closely coincident with NLDN strokes. The example shown in Figure 1 has had its amplitude artificially reduced in some rows (frequencies) to suppress interfering communication carriers [*Jacobson et al.*, 1999]. Moreover, in the top half of the spectrum (i.e, above 37 MHz), the two magnetic-birefringence modes are insufficiently resolved to prevent their mutual interference [*Jacobson and Shao*, 2001]. However, the lower third of the spectrum (below 34 MHz), in which there is good mode separation, and in which the prewhitening has not corrupted the amplitudes, shows a very steady signal spectral density (in each mode) as a function of frequency. This covers 6 MHz of bandwidth in which the signal doesn't fade noticeably versus frequency.

VHF emissions are usually thought to occur because of very fast processes occuring in the growth and propagation of leader tips in "virgin air". These emission sources could occupy a finite volume and would consist of many spatially and temporally unsynchronized elementary emitters. How big is the VIP emission source, if the source consists of a spatially extended ensemble of mutually independent emitters? There are two estimates we can make, the first based on pulsewidth, and the second on coherence bandwidth. The first estimate is simply the pulse width times *c*, the speed of light. This would yield a dimension of 200 m or less; this is an upper bound. The second estimate is as follows: The theory of partial coherence [*Born and Wolf*, 1975] tells us that the range of distances from the satellite to the emission source, considering the entirety of the emission source, must not exceed the speed of light divided by the fading bandwidth. This is $c/(6X10^6\ s^{-1})$, or about 50 m. Barring some fortuitous orientation of the source, this suggests that the characteristic source size is also on the order of 50 m. Moreover, we suspect that the true coherence bandwidth exceeds 7 MHz, but in this example the fading bandwidth is not readily determinable above that limit, due to the interference fading

between unresolved modes. Thus the true emission source size may be closer to 15 m than to 50 m.

By any standard, an intracloud transient lightning radiation source of dimension only 15-50 m is rather unusual. A leader progressing between opposite intracloud charge regions would have to traverse a much greater distance, on the order of a km or more. Moreover, such a leader would exhibit multiple recurrences of VHF emission within the leader lifetime, up to a fraction of a second. By contrast, in the case of VIPs we generally do not see neighboring VIPs occuring within a leader lifetime. *Therefore, it is likely that the process responsible for VIPs is not a classic intracloud leader.*

The types of VHF signals that are closely coincident with NLDN tend to fall into a few simple classes, as shown in Figure 2. Each panel is a spectrogram showing spectral density both versus time during 40 μs centered on the pulse (horizontal axis) and versus frequency in the entire low-band frequency range (vertical axis). The Fourier temporal resolution in Figure 2 is on the order of 0.3 μs, half that of Figure 1. The following are the exemplar signal types in Figure 2:

The upper-left panel in Figure 2 shows a typical VHF signature associated with negative cloud to ground (-CG) attachment to the sea, or NCGS for short (discussed in regard to Figure 4 a, below). The intrinsic pulse width of the NCGS signal (either ordinary or extraordinary mode) is no greater than the measurement limit of 0.3μs. The NCGS signature is typically highly coherent, even moreso than the VIP signature (see above). Indeed, the partial-coherence argument suggests a dimension of 15 m for the NCGS source (if the source consists of an ensemble of incoherent emitters), because the fading bandwidth approaches 20 MHz. Alternatively, the VHF signal might be due to simple dipole radiation from the single organized stalk of negative vertical current whose risetime over seawater is known to be typically in the range 60 - 70 ns [*Willett et al.*, 1990; *Willett et al.*, 1998].

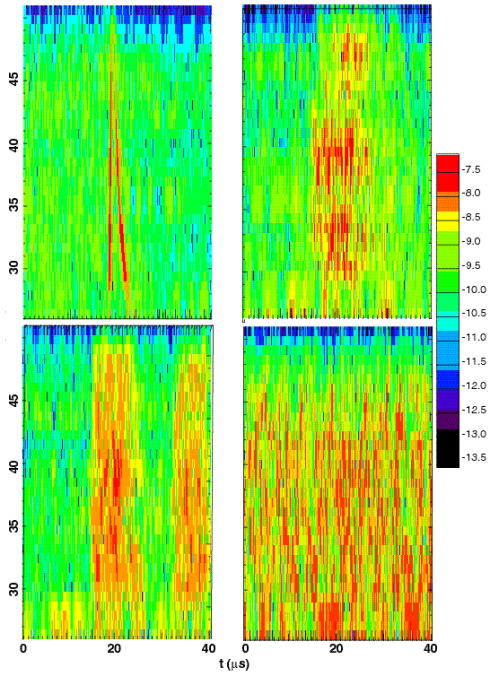

Figure 2: Spectrograms of power spectral density versus frequency (vertical axis) and time (horizontal axis) for four prototypical VHF event types that can be closely coincident with NLDN stroke times. The color scale is the $\log_{10}$ of square of the received electric field. Upper left: VHF coherent transient associated with negative cloud-to-ground stroke on seawater ("NCGS"); upper right: incoherent monopulse; lower left: incoherent, wide pulse pair; lower right: incoherent broad emission. All data have been both prewhitened and first-order dechirped (see text). The Fourier window is 64 samples (1.28 μs) and is slid forward by 4 samples (80 ns). The weighting function within the 64-sample window provides an effective time resolution of about 300 ns.

The upper-right panel in Figure 2 shows a single pulse, or possibly a pulse pair with unresolved time-of-flight splitting. The intrinsic width is on the order of 5 - 15 μs, and the signature has a very small fading bandwidth. These two facts are consistent with large (~km) spatial dimension, much larger than either VIP or NCGS source dimensions. This signature can closely coincide with the whole gamut of NLDN strokes.

The lower-left panel of Figure 2 shows a resolved pulse-pair, each pulse consisting of a wide and perfectly incoherent signal (such as the monopulse in the upper-right panel.) Like the monopulse, this signature can closely coincide with the whole gamut of NLDN strokes.

Finally, pulses resembling those of the upper-right and lower-left panels can become even broader (>20 μs) such that a ground reflection is decreasingly likely to be distinguished, even if the pulse is emitted from an elevated height above the ground. This kind of signal is shown in the lower-right panel of Figure 2. The fading bandwidth of such signals is negligible, consistent with very large source dimensions, relative to either VIPs or NCGSs.

Reviewing the signals in Figure 2, the only forensically unique telltale of a well-determined counterpart NLDN stroke is the NCGS. Apart from the NCGS, the signals which are closely coincident with the whole gamut of NLDN strokes do not readily discriminate between those associated strokes. Reviewing the null result which we treated first, the VIP signature almost always marks a transient, punctual breakdown which is temporally unrelated to NLDN strokes and which tends not to time-cluster into “flashes”.

Altogether, locations of the 27,756 closely-coincident NLDN strokes from the two 6-month campaigns are shown in Figure 3. The color codes the stroke type: Red is IC, green is negative CG, blue is positive CG, and black is any stroke whose distance from the nearest NLDN station is great enough (>625 km) to preclude stroke-type identification [*Jacobson et al.*, 2000].

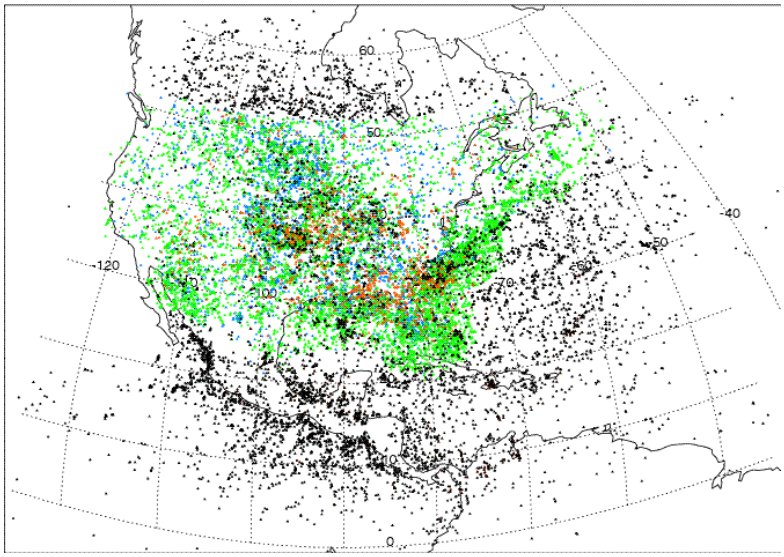

Figure 3: Locations of all 25,756 NLDN strokes that have closely coincident FORTE VHF counterparts. The color codes the stroke type: Red is IC, green is negative CG, blue is positive CG, and black is any stroke whose distance from the nearest NLDN station is great enough (>625 km) to preclude stroke-type identification.

(3b) Systematics of the submicrosecond transient accompanying -CG strokes

As stated above in the discussion of the upper-left panel in Figure 2, there is often a very narrow VHF transient associated with NLDN negative CG strokes. In order to search

systematically for these events' occurences, we employ an automated data-reduction algorithm that examines indifferently the VHF data from all 25-thousand closely coincident events. The algorithm estimates the power-weighted signal duration and attempts, with some success, to recognize birefringent splitting and then make the width estimate on the basis of just one propagation mode's individual signal. The algorithm selects for width < 0.4 μs, as well as for a signal-to-noise threshold. Later visual inspection of the algorithm's decisionmaking indicates to the authors that the algorithm's positive selections are correct at the 95% level, but that the missed positives constitute up to 50% of the events in the 25-thousand-event parent population. In other words, the events which *are selected* are done so with only ~1 false selection in 20, but there are many events which are *not selected* which should have been.

This moderate-false-positive, high-false-negative automated selection algorithm chooses 2411 narrow VHF transients, whose positions and stroke types (encoded in color) are shown in Figure 4. These 2411 strokes constitute about 10% of all the 25-thousand closely coincident events. Almost all of the selected events are negative CGs. Moreover, the vast majority of the selected events are over seawater. This is the reason we choose to call these VHF events NCGSs, even if there are a few of them on continents, at least nominally according to the robotic algorithm. Of all events at sea for which NLDN can provide a type, the fraction which are nominal NCGSs is 0.16. For land, that ratio is 0.037.

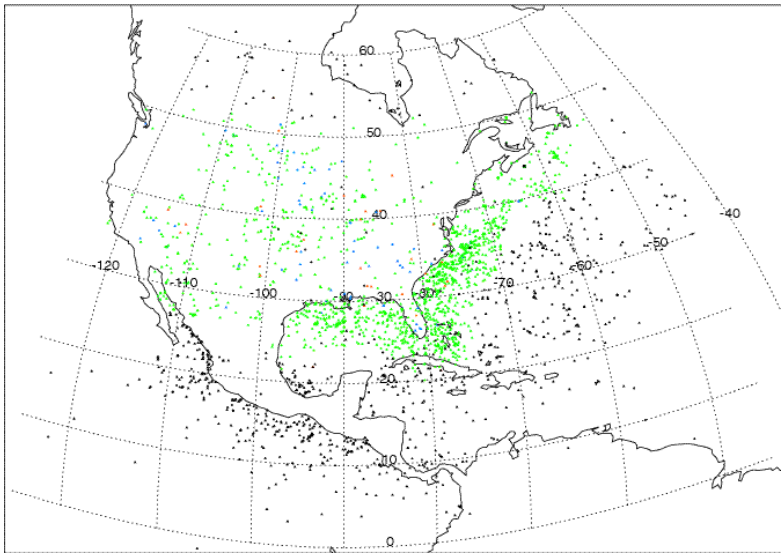

Figure 4: Locations of the 2411 NLDN strokes that pass the automated criteria for narrowness and lack of fading typical of NCGS's. Color as in previous Figure.

(3c) FORTE-coincident versus contemporaneous background NLDN strokes

Our initial description of the first FORTE/NLDN joint campaign [*Jacobson et al.*, 2000] treated "background" NLDN strokes as those which occurred within ±0.2 s of closely-coincident strokes. This tended to include an admixture of strokes in the same flashes as those containing closely coincident strokes, as well as strokes in merely the same storms as those containing closely coincident strokes, and finally a few strokes from storms which entirely lacked closely coincident strokes.

In what follows, we treat the contemporaneous background of NLDN strokes in a more natural and predictable way. We take the entire twelve months of NLDN stroke data and select all epochs during which FORTE was within view of somewhere in the North America sector. Next, we down-select these strokes to include only those strokes for which (1) FORTE was contemporaneously above the local horizon (reckoned from the stroke), and (2) FORTE's radio-frequency digitizer was armed and collecting data. This final selection provides a list of all those NLDN strokes associated with which FORTE had the opportunity and ability, in principle, to observe VHF signals.

We wish to relate NLDN stroke characteristics (type, peak vertical current) to the associated FORTE observations. Since the long-range NLDN-detected strokes (the black symbols in Figures 3 and 4) lack both type and peak vertical current estimates, we will exclude them (and their associated FORTE events) from the rest of this subsection.

Table 1 summarizes the overall results for each characterized NLDN stroke type (negative CC, positive CG, and IC) for both land and sea locations. Not surprisingly, most NLDN stroke detections (in all these categories) are over land, because the array is situated on the continent and has finite range (<625 km for this down-selected data set). Also not surprisingly, most NLDN strokes are -CGs, because (especially over sea) that is in general the dominant ground stroke type [*Orville*, 1994]. The new result in Table 1 is the difference in likelihood of FORTE close coincidence for NLDN-detected strokes over land versus over sea water: For -CG strokes, those over sea are almost five times more likely to be closely coincident with FORTE, compared to those over land. For +CG strokes, the enhancement is more than two-fold. For IC strokes, the enhancement is three-fold.

It has been shown in an earlier publication [*Jacobson et al.*, 2000] that there is a tendency for enhanced FORTE VHF detection of strokes that are higher in NLDN-inferred peak current. Considering that the maritime strokes in Table 1 are all in the marginal range for detection by NLDN [*Cummins et al.*, 1998], it seems likely that the vertical-current distribution *for strokes detected over the ocean by NLDN* might be higher than the current of NLDN-detected continental strokes. This could contribute to the dramatic maritime-versus-continental enhancement of a closely coincident FORTE VHF detection.

Figure 5 compares the distribution of NLDN-inferred peak current amplitude of -CG strokes for land (solid curves) and sea (dashed curves). The top panel is for all contemporaneous background NLDN strokes. The lower panel is for the subset of NLDN strokes that have closely coincident FORTE events. As expected on the basis of detection considerations, the contemporaneous background NLDN strokes (upper panel) over the sea tend to be higher-current than are those over the land. Moreover, the distributions of

current for the strokes closely coincident with FORTE VHF events (lower panel) are wider and are skewed toward higher current.

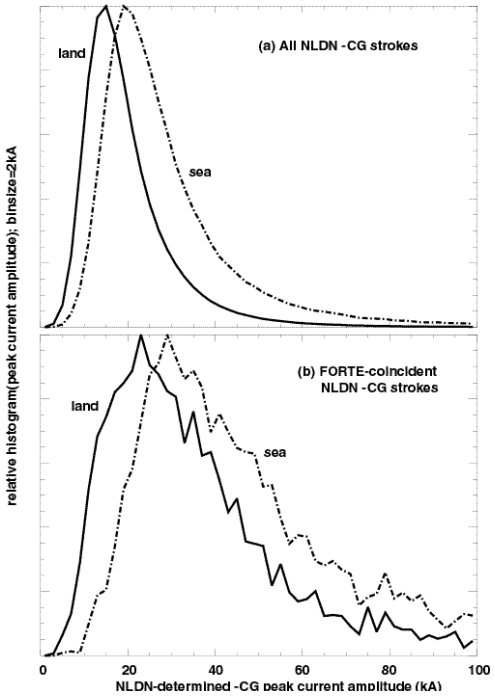

Figure 5: Distributions of peak-current amplitude (as determined by NLDN) for (a) the entire contemporaneous NLDN background -CG strokes accessible by FORTE and (b) the subset of NLDN -CG strokes that are closely coincident with FORTE VHF events. Solid: strokes over land; dashed: strokes over the sea.

Figure 6 is similar to Figure 5 but pertains to +CG strokes. We note an obvious difference between the land-versus-sea FORTE coincidence statistics for +CG strokes as compared to -CG strokes: Although the contemporaneous background NLDN-inferred stroke currents tend to be higher over sea than over land for both -CG and +CG strokes , the FORTE-coincident subclass of +CG strokes (lower panel of Figure 6) does *not* show as much of a higher current over sea (as opposed to land). This is in contrast to the behavior of -CG strokes (see Figure 5, lower panel).

(3d) Storm-grouping statistics

It is apparent from the FORTE VHF and NLDN correlations, and more importantly from the frequent *lack* of correlations, that these two lightning-detection systems are sensitive to complementary aspects of thunderstorm electrification and lightning. We need to examine the relationship between FORTE VHF detection of overall lightning storms in the light of NLDN characterization of those storms. Therefore it is advisable to define

storm clusters of NLDN-detected strokes and then to determine the factors influencing how many closely coincident FORTE VHF events are found for that storm. This will result in an under-estimate of FORTE's VHF detection rate for that storm, of course, because there are many FORTE VHF events which are wholly uncorrelated with NLDN. These latter FORTE VHF events will be discussed in terms of case examples in Section 4 below.

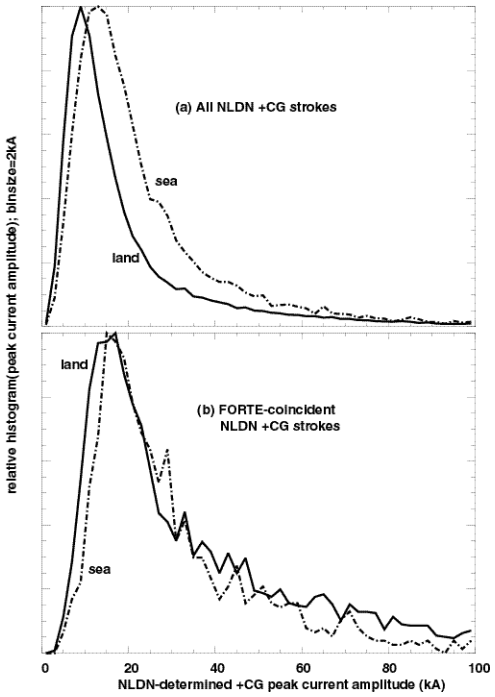

Figure 6: Similar to Figure 5, but for +CG strokes.

During the 12 months of cumulative FORTE/NLDN campaigns, FORTE performed 2135 orbital passes in view of North America in which (1) NLDN-reported stroke locations were geometrically visible to FORTE, and (2) FORTE was armed and recording signals. Within the 2135 FORTE passes in which NLDN strokes were visible, the per-pass stroke set was placed onto a map in 1degX1deg location bins, on 1/2 deg X 1/2 deg centers (50% overlap). Then, whenever a pass/location cell registered >20 NLDN strokes that were geometrically visible to FORTE, that pass/location was registered as a "storm". Cumulatively, there were 17,437 such "storms". These "storm" clusters of NLDN events *do not* correspond one-to-one with physically meaningful thunderstorm or thundercell structures, in contrast to the more physically meaningful storm correspondence that was

accomplished with TRMM/LIS optical data [*Boccippio et al.*, 2001]. Rather, the present clustering of NLDN strokes into “storms” is only a convenience for exploring the correlated VHF detection by FORTE. Its physical meaning in terms of thunderstorms or thundercells is only approximate.

Figure 7 shows the positions of the NLDN-detected storms within each of which the majority of strokes are characterizable by NLDN as -CG, +CG, or IC. This corresponds roughly to those storms whose distance to the nearest NLDN sensor does not exceed 625 km [*Jacobson et al.*, 2000]. The number of such characterizable storms is 16,625. These storms tend to occur near the SE United States and adjacent coastal areas. For each storm, the location shown in Figure 7 is the stroke-weighted location, which can vary within the regular cell grid, depending on the contemporaneous NLDN stroke locations within that grid cell.

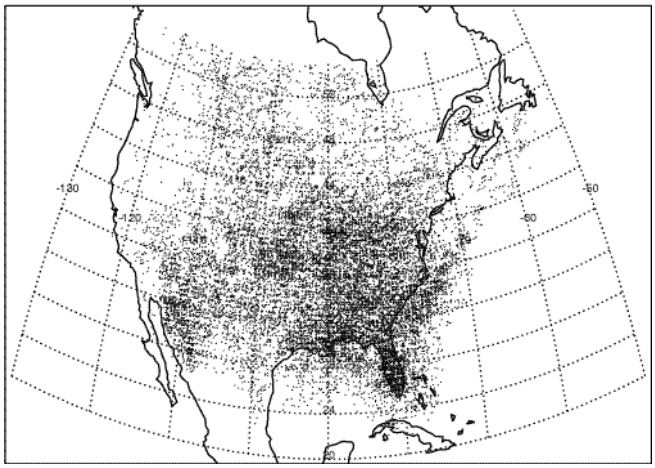

Figure 7: Location of “storms” in the NLDN contemporaneous background (see text), limited to strokes types -CG, +CG, and IC.

For the 16,625 NLDN characterizable storms accessible to FORTE VHF (though not necessarily detected by FORTE), Figure 8 shows the normalized distributions of the +CG fraction within the storm, for all storms as defined above. This statistic is the fraction of strokes (determined by NLDN to be -CG, +CG, and IC) that are determined by NLDN to

be +CG. Note that the vertical scale is logarithmic. Data over land are in the solid curve, and data over sea are in the dashed curve. As noted earlier, the vast majority of NLDN-characterized storms are dominated by -CG strokes, because that is usually the preferred polarity for thunderstorms. Figure 8 shows that the +CG fraction over land is greater than over sea.

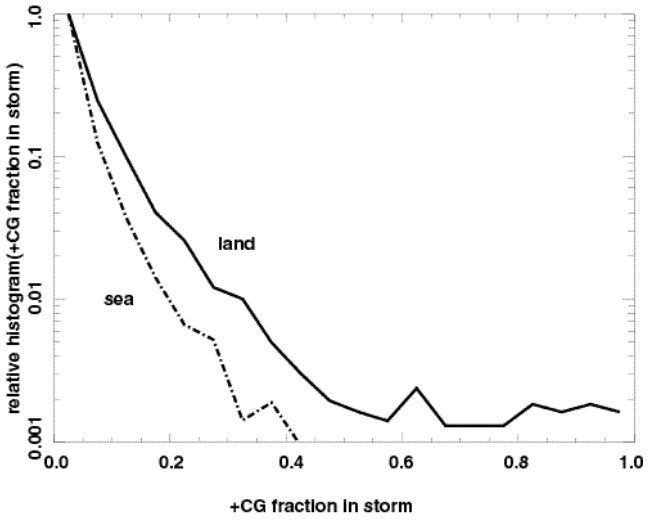

Figure 8: Separately-normalized histograms of the fraction of strokes that are +CG in each storm shown in previous figure. Solid curve is for storms over land; dashed, for sea. Vertical scale is logarithmic.

Figure 9 shows the distribution of the fraction of storm strokes that are closely coincident with FORTE VHF. Data over land are in the solid curve, and data over sea are in the dashed curve. Note that the vertical scale is logarithmic. The statistics are gathered only over the 16,625 NLDN characterizable storms accessible to FORTE. Evidently the storms over sea have a higher fraction of strokes that are closely coincident with FORTE VHF events, at least in the distibutions' tail behavior. We reiterate that the FORTE VHF storm-detection efficiency implied in Figure 9 takes account only of those FORTE VHF events which are closely coincident with NLDN-characterized strokes. This is a gross under-estimate of the total possible number of FORTE VHF events associated with an NLDN-detected storm (see Section 4 below).

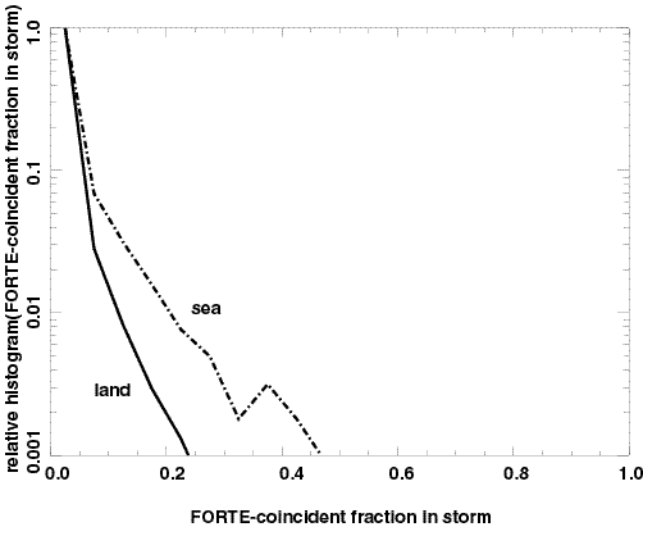

Figure 9: Similar to Figure 8, but showing the fraction of strokes in each storm that are closely coincident with FORTE VHF events.

Figure 10 is a bar-chart of the fraction of strokes in each *land-based* storm which are closely coincident with FORTE VHF events, as a function of the fraction of strokes in that storm that are +CG. The binning is in steps of 0.2 on the abscissa. The ordinate is averaged over all land-based storms within each abscissa bin. The clear result is that land-based storms with increasing +CG fraction are also increasingly likely to have strokes which are closely coincident with FORTE VHF events. However, there are so few storms with significant +CG fraction (see Figure 8 above) that the right half of Figure 10 is mainly about the distribution's tail. Nonetheless the point is clear, that more positive CGs means more FORTE closely-coincident VHF events, at least over land. (There are not enough +CG strokes over water to permit doing the analysis of Figure 10 for maritime storms.)

(4) FORTE/NLDN campaign case example

The statistical probability of closely coincident FORTE VHF and NLDN LF/VLF detections of the same "stroke" is very small, as shown in Section 3. This does not mean, however, that FORTE misses the storms that lack closely coincident FORTE VHF and NLDN LF/VLF events. Rather, the vast majority of FORTE VHF events, even when FORTE is in view of NLDN storms, are from storm processes that are not closely

coincident in time with strokes detectable by NLDN. Unfortunately, these non-closely-coincident FORTE VHF events cannot be individually geolocated, although an ensemble of them from a common storm can in some cases be given an inferred location [*Jacobson et al.*, 1999; *Jacobson and Shao*, 2001; *Tierney et al.*, 2001].

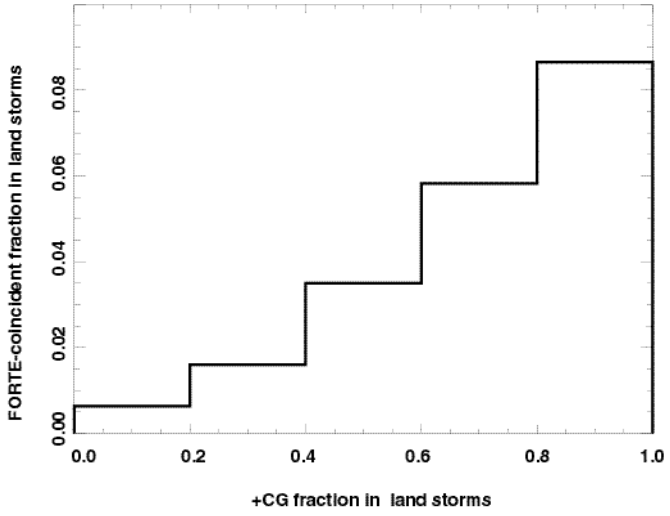

Figure 10: Bar-chart of mean fraction of strokes that are closely coincident with FORTE VHF events, in successive bins of the fraction of strokes that are +CG .

Being just one satellite, FORTE is incapable of single-event geolocation of VHF sources. While a constellation of satellites can, in principle, perform multi-satellite differential time-of-arrival location[*Suszcynsky et al.*, 2000a], a single satellite cannot. Therefore, most FORTE VHF events lack sure geolocation. Given this reality, it is somewhat difficult to deduce from FORTE data a final conclusion about the storm-detecting efficiency of a space-based constellation of lightning VHF lightning monitors [*Suszcynsky et al.*, 2000a].

Despite this very obvious deficiency of a single-satellite VHF lighning dataset, we can in some cases “borrow” the NLDN-furnished geolocation from a closely-coincident FORTE VHF event and use it for other VHF events of what are likely to derive from the same storm [*Tierney et al.*, 2001]. This allows us to see how FORTE detects VHF signals from a given storm selected for study.

To illustrate this, we choose a FORTE satellite pass in view of eastern North America starting around 0 UT on 20 August 1999. Figure 11 shows (blue squares) the subsatellite points at which the FORTE VHF system triggered and collected records. Also shown (red squares) are the locations of NLDN strokes that are closely coincident with certain FORTE VHF events. Each pair of NLDN stroke and FORTE-subsatellite location are connected by a blue line. Finally, the contemporaneous NLDN stroke background for this satellite-pass is shown in green. The latter are highly overlapped on this course spatial resolution but at least provide a rough location of where relevant, FORTE-accessible lightning activity is occuring. Several storms in Figure 11 have FORTE closely-coincident VHF events. Here we shall study the FORTE detections of storms “a” and “b”, respectively in South Carolina and off the South Carolina coast.

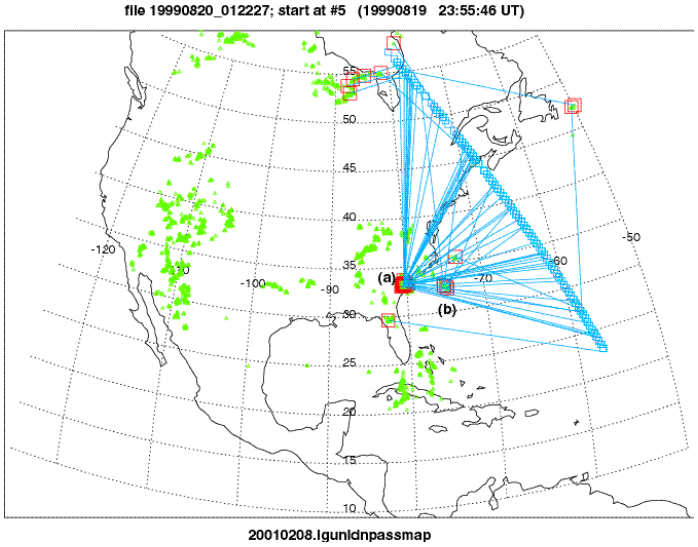

Figure 11: Map of a descending satellite pass within view of contemporaneous NLDN background strokes (shown in green, regardless of stroke type). For each close coincidence between an NLDN stroke and a FORTE VHF event, the stroke location is circumscribed by a red square, the subsatellite location is marked by a blue square, and each corresponding pair is connected by a blue line.

Figure 12 shows closeup views of the two selected storms’ NLDN stroke sets. The background NLDN strokes are marked as dots if they lack a FORTE VHF closely-coincident event. On the other hand, if there is a closely-coincident FORTE VHF event, the stroke is marked as a small black triangle circumscribed by a larger, outer triangle.

Both the dots (for non-closely-coincident strokes) and the outer triangles (for closely-coincident strokes) are color-coded for stroke type (green=-CG, blue=+CG, and red=IC). The striking difference between these two storms in Figure 12 is the several-fold-higher number of both NLDN background and NLDN closely-coincident events in storm (a) then in storm (b). Table 2 give the counts of various NLDN events in the two storms, as well as probabilities of there being closely coincident FORTE VHF events.

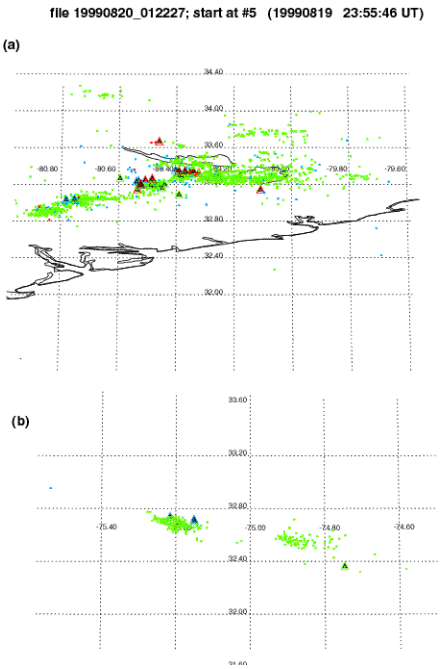

Figure 12: Expanded view of the two storms marked “a” (continental) and “b” (marine) in previous figure. The color codes the stroke type: Red is IC, green is negative CG, and blue is positive CG. Each stroke that is closely coincident with a FORTE VHF event is further highlighted by a larger triangle (with same color coding) and an inscribed black triangle.

Figure 13 shows the peak vertical current for each of the NLDN strokes in storm “a” (top panel) and in storm “b” (bottom panel). Black and colored triangles mark the strokes that are closely coincident with FORTE VHF events. The color coding is unchanged (green=negative CG, blue=positive CG, and red=IC).

The continental storm in Figure 13(a) has a significant minority of +CG and IC strokes, and these are more likely than are the -CGs to be closely-coincident with FORTE VHF. The +CG strokes are generally low-current compared to the highest-current -CG strokes. Most of the -CG strokes that have FORTE VHF close coincidences are relatively high current, in the range 50-130 kA. By comparison, the marine storm in Figure 13(b) has

only four strokes that are not -CGs, and all but one of these has a FORTE VHF close coincidence. There are only two -CG strokes with FORTE VHF close coincidences.

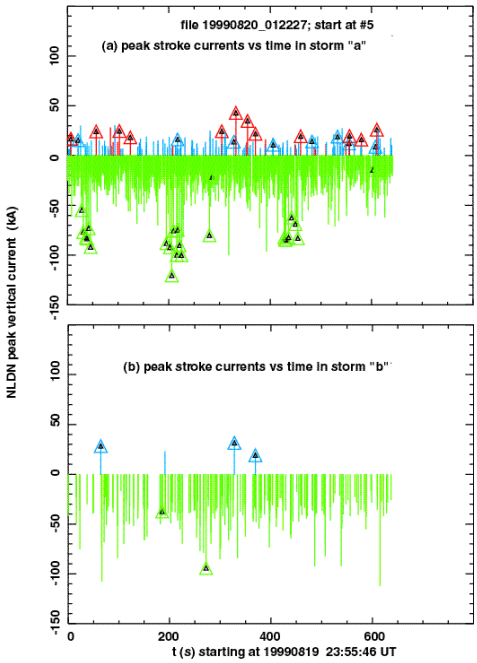

Figure 13: Peak vertical current versus time for (a) the continental and (b) the marine storms of previous figures. The color codes the stroke type: Red is IC, green is negative CG, and blue is positive CG. Each stroke that is closely coincident with a FORTE VHF event is further highlighted by a larger triangle (with same color coding) and an inscribed black triangle.

The close-in data of Figures 12 and 13 indicate that for both NLDN strokes and NLDN/FORTE VHF coincidences, the continental storm (a) is better detected than is the maritime storm (b). However, when we look at the non-NLDN-coincident FORTE VHF data and make a reasonable association of those events to either of these storms, we will see that there are several-fold more FORTE VHF detections of the marine storm (b) than of the contintental storm (a).

It has been shown elsewhere [*Jacobson et al.*, 1999; *Tierney et al.*, 2001] that the total electron content (TEC) along the line-of-sight from a lightning storm to FORTE can be used to group strings of FORTE events into quasi-discrete storms. Essentially, the slant pathlength of the line-of-sight through the ionosphere controls the TEC deduced from the plasma dispersion in any single event's data. The TEC is minimum at closest approach, where the satellite elevation angle (see from the storm) is maximum. The TEC increases as the satellite elevation angle decreases. Thus a record of TEC versus time during a

satellite pass begins with high TEC, undergoes reduced TEC as the elevation angle increases, reaches a minimum TEC at maximum elevation angle, and then undoes this progress as the satellite elevation angle gets smaller again [*Jacobson et al.*, 1999].

Figure 14 (a) shows the TEC inferred from signal dispersion [*Jacobson et al.*, 1999] versus time during about 11 minutes of the satellite pass of Figures 11-13. Any FORTE VHF event with a closely coincident NLDN sferic has its square TEC symbol surrounded by a diamond symbol. In addition to a jumble of irregularly-placed TEC values in Figure 14 (a), there are two clear TEC trends whose character has been shown to indicate quasi-localized storms. The markings (a) and (b) correspond to the continental and marine storms of Figures 12 and 13. Early in the satellite pass (see Figure 11), both these storms are roughly equidistant from FORTE, and accordingly the two storms' TEC trends are initially blended together. Later in the pass, however, FORTE becomes closer to storm (b) than to storm (a), resulting in a higher FORTE elevation angle as seen from storm (b) compared to storm (a). This causes the two TEC trends to separate, with the TEC for storm (b) events becoming smaller than the TEC for contemporary storm (a) events.

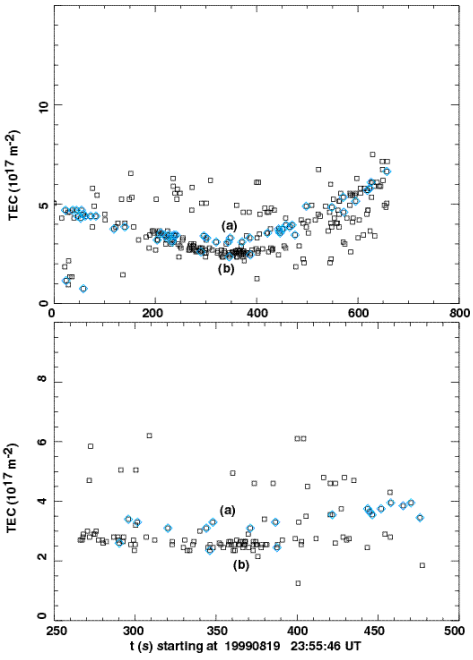

Figure 14: TEC (slant total electron content) versus time for FORTE VHF events in the satellite pass of previous figures. Those events highlighted with diamond symbols are closely coincident with NLDN strokes. (a) Entire pass; (b) closeup of 260-480 s during the pass.

During the time region 260 through 480 sec in Figure 14(a), it is possible to discriminate between events belonging to the two major storms, on the basis of TEC. This time epoch is shown in Figure 14 (b). In addtion to the two major storms (a) and (b), there are two unassociated VHF events at lower TEC than storm (b), and there are many unassociated events at higher TEC than storm (a). We will ignore those VHF events that are unassociated with either storm (a) or storm (b). We use the TEC trends in Figure 14 (b) to identify 24 VHF events whose origin is storm (a) and 62 VHF events whose origin is storm (b).

Figure 15 shows the VHF power-versus-time profiles for the 24 VHF events whose origin is storm (a). Each profile is obtained by prewhitening and then dechirping [*Jacobson et al.*, 1999] the received electric field, prior to squaring to obtain a signal proportional to power. All the profiles are separately scaled to have approximately the same peak height, for comparison. Each profile is marked with the sequential event number within the parent raw-data file. Those VHF power profiles whose events have closely-coincident NLDN strokes are noted with both the stroke type ("G for ground stroke, and "C" for intracloud stroke) and the stroke peak current (signed for either -CG or +CG).

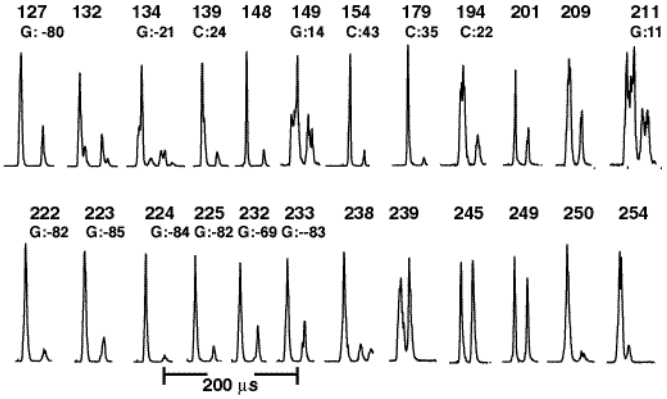

Figure 15: Profiles of power versus time, after prewhitening and dechirping, for the VHF signals in the continental storm "a". Each profile has been separately normalized to show its shape. Only the active part of each VHF record is included. Each profile is labeled by the sequence number within the raw-data file. Below the sequence number, the associated stroke type and peak vertical current are noted for those VHF events that are closely coincident with NLDN strokes.

All the power profiles in Figure 15 for the continental storm converge on the pulse-plus-ground-reflection (pulse pair) paradigm (see Figure 2, lower-left panel), regardless (in the case of those whose associated stroke is noted) of the type (-CG, +CG, or IC) of closely-coincident NLDN stroke. In part this is due to the higher power of broad pulse pairs compared to most other types of VHF signals detected by FORTE; higher power means higher detectability from orbit. In part, also, the prevalence of pulse pairs in the FORTE data is due to the ease of triggering on a signal whose power is of relatively short duration [*Jacobson et al.*, 1999].

For whatever reason, the dominant manifestation of lightning seen by the FORTE VHF receivers tends to be pulse pairs when the receiver is autonomously triggered, as opposed to either (a) being triggered externally by the optical signal [*Light et al.*, 2001] or (b) being required to coincide with an independently triggered optical signal [*Suszcynsky et al.*, 2000b]. Being a pulse pair means that the origin is perforce an intracloud breakdown, and (insofar as the storm location is known) this allows retrieval of the emission height (as will be discussed in connection with Figure 17 below). *With regard to Figure 15, even though many of the associated strokes are CGs, the FORTE VHF is uniformly due to an associated intracloud process.*

Figure 16 is similar to Figure 15, but for the maritime storm (b). There are only two events whose power profiles do not fit the pulse-pair paradigm. The first of these non-pulse-pair events (#123) is an NCGS signal (see Section 3(b) above) with significant leader noise preceding the coherent peak. The second non-pulse-pair (#146) is an extended incoherent emission closest in type to the last example (lower-right panel) of Figure 2. *All the 62 other FORTE VHF signals from the maritime storm are pulse pairs.* The pulse pair (#180) that we can associate with a +CG is not distinguishable from other pulse pairs. Thus, with the exception mainly of distinctive NCGS signals (predominantly associated with the transient startup of a negative return stroke over salt water), *the VHF signals in the marine storm are also dominantly of intracloud origin.*

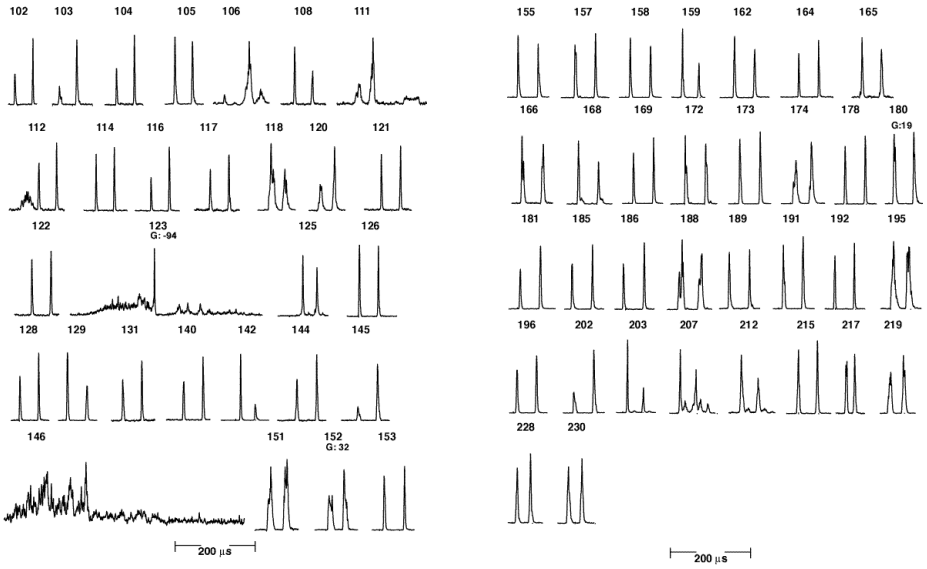

Figure 16: Similar to Figure 15, but for the marine storm “b”.

Given that most of the events in these two storms are pulse pairs, we can retrieve the pulse-emission height above ground for those events [*Jacobson et al.*, 1999]. Figure 17 shows the retrieved emission heights for both storms. Clearly they both show a bi-level emission pattern, as has been noted by ground-based observations [*Shao and Krehbiel*, 1996]. The heights of the levels are roughly comparable between the two storms, although the levels are much more evident in the marine storm.

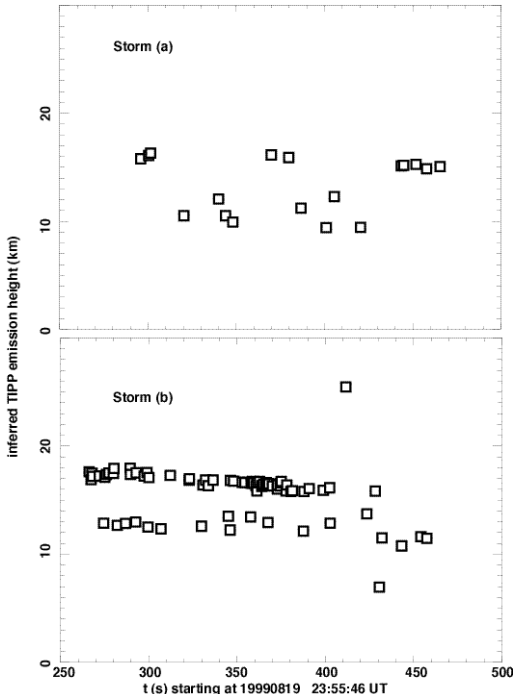

Figure 17: Inferred VHF emission height versus time for (a) continental storm "a" and (b) marine storm "b" (see text).

5. Discussion

The pair of storms, one continental and the other maritime, that we have discussed in Section 4 section are quite typical of the entire collection of storms seen by FORTE VHF. This leads to the insight that the dominance of pulse-pair power profiles (and hence of an intracloud emission process) typefies most FORTE VHF data from lightning, at least when the VHF receiver is autonomously triggered. *An intracloud emission source provides the dominant VHF observable, even when the associated NLDN closely coincident stroke is nominally a ground return stroke.* An important exception to this is the systematic appearance of NCGS VHF signatures emitted from near the seawater surface during the initiation of a -CG return stroke at sea. The fact that FORTE sees VHF manifestations of intracloud emissions, even during nominal ground strokes, is not ruled out by the literature. For example, ground-based, VHF interferometric observations [*Shao et al.*, 1995] show that a "ground stroke" is accompanied by a rich assortment of processes at altitude, as the entire system is electrically coupled through all altitudes in the storm, even though NLDN is (by design) preferentially likely to detect simply the ground return stroke.

Another insight from this case study, and from its representativeness of most FORTE VHF observations of lightning storms, is that VHF lightning signatures alone tend to provide little obvious discrimination (in the power profile) between IC, +CG, and -CG processes, at least over continents. Rather, the dominant VHF signature tends to be a pulse pair (in-cloud VHF emission, plus a delayed ground reflection.) Over oceans this is still basically true, although there is the added possibility of a coherent VHF pulse originating near the sea surface during initiation of negative return strokes. By contrast, the VHF signatures of various lightning strokes show a systematic utility in classifying those strokes when the VHF trigger is derived from the co-located optical sensor aboard FORTE, i.e. when the VHF is not autonomously triggered [*Light et al.*, 2001], or when the VHF is required to coincide with an independently triggered optical signal [*Suszcynsky et al.*, 2000b].

Finally, we note an important class of FORTE signals, the narrow and relatively coherent "VIP" pulse pairs, that tend not to be associated at all with NLDN strokes.

References

Boccippio, D.J., K.L. Cummins, H.J. Christian, and S.J. Goodman, Combined satellite- and surface-based estimation of the intracloud-cloud-to-ground lightning ratio over the Continental United States, *Mon. Weath. Rev.*, *129*, 108-122, 2001.

Boccippio, D.J., S.J. Goodman, and S. Heckman, Regional differences in tropical lightning distributions, *J. Appl. Meteor.*, *39*, 2231-2248, 2000.

Born, M., and E. Wolf, *Principles of Optics*, Pergamon Press, Oxford, 1975.

Cummins, K.L., M.J. Murphy, E.A. Bardo, W.L. Hiscox, R. Pyle, and A.E. Pifer, Combined TOA/MDF technology upgrade of U. S. National Lightning Detection Network, *J. Geophys. Res.*, *103* (D8), 9035-9044, 1998.

Holden, D.N., C.P. Munson, and J.C. Devenport, Satellite observations of transionospheric pulse pairs, *Geophys. Res. Lett.*, *22* (8), 889-892, 1995.

Jacobson, A.R., Recent results from the FORTE RF payload, in *11th International Conference on Atmospheric Electricity*, edited by H. Christian, pp. 668-671, NASA, Global Hydrology and Climate Center, NASA Marshall Space Flight Center, Huntsville, Alabama, 1999.

Jacobson, A.R., K.L. Cummins, M. Carter, P. Klingner, D. Roussel-Dupré, and S.O. Knox, FORTE radio-frequency observations of lightning strokes detected by the National Lightning Detection Network, *J. Geophys. Res.*, *105* (D12), 15,653, 2000.

Jacobson, A.R., S.O. Knox, R. Franz, and D.C. Enemark, FORTE observations of lightning radio-frequency signatures: Capabilities and basic results, *Radio Sci.*, *34* (2), 337-354, 1999.

Jacobson, A.R., and X.-M. Shao, Using geomagnetic birefringence to locate sources of impulsive, terrestrial VHF signals detected by satellites on orbit, *Radio Science*, *in press*, 2001.

Light, T.E., D.M. Suszcynsky, and A.R. Jacobson, Coincident Radio Frequency and Optical Emissions from Lightning, Observed with the FORTE Satellite, *J. Geophys. Res.*, *submitted,* 2001.

Massey, R.S., and D.N. Holden, Phenomenology of transionospheric pulse pairs, *Radio Sci.*, *30* (5), 1645-1659, 1995.

Massey, R.S., D.N. Holden, and X.-M. Shao, Phenomenology of trans-ionospheric pulse pairs: Further observations, *Radio Sci*, *33*, 1755-1761, 1998a.

Massey, R.S., S.O. Knox, R.C. Franz, D.N. Holden, and C.T. Rhodes, Measurements of transionospheric radio propagation parameters using the FORTE satellite, *Radio Sci.*, *33* (6), 1739-1753, 1998b.

Orville, R.E., Cloud-to-ground lightning flash characteristics in the contiguous United States, *J. Geophys. Res.*, *99* (D5), 10,833-10,841, 1994.

Petersen, W.A., and S.A. Rutledge, On the relationship between cloud-to-ground lightning and convective rainfall, *J. Geophys. Res.*, *103* (D12), 14,025-14,040, 1998.

Proctor, D.E., VHF radio pictures of cloud flashes, *J. Geophys. Res.*, *86* (C5), 4041-4071, 1981.

Proctor, D.E., R. Uytenbogaardt, and B.M. Meredith, VHF radio pictures of lightning flashes to ground, *J. Geophys. Res.*, *93* (D10), 12,683-12,727, 1988.

Rhodes, C.T., X.M. Shao, P.R. Krehbiel, R.J. Thomas, and C.O. Hayenga, Observations of lightning phenomena using radio interferometry, *J. Geophys. Res.*, *99*, 13059-13082, 1994.

Shao, X.-M., C.T. Rhodes, and D.N. Holden, RF radiation observations of positive cloud-to-ground flashes, *J. Geophys. Res.*, *104* (D8), 9601-9608, 1999.

Shao, X.M., and P.R. Krehbiel, The spatial and temporal development of intracloud lightning, *J. Geophys. Res.*, *101* (D21), 26,641-26,668, 1996.

Shao, X.M., P.R. Krehbiel, R.J. Thomas, and W. Rison, Radio interferometric observations of cloud-to-ground lightning phenomena in Florida, *J. Geophys. Res.*, *100* (D2), 2,749-2,783, 1995.

Suszcynsky, D., A. Jacobson, J. Fitzgerald, C. Rhodes, E. Tech, and D. Roussel-Dupre, Satellite-based global lightning and severe storm monitoring using VHF receivers, *EOS, Trans. Am. Geophys. Union, 81* (48), F91, 2000a.

Suszcynsky, D.M., T.E. Light, S. Davis, M.W. Kirkland, J.L. Green, and J. Guillen, Coordinated Observations of Optical Lightning from Space using the FORTE Photodiode Detector and CCD Imager, *J. Geophys. Res., submitted*, 2000b.

Taylor, W.L., A VHF technique for space-time mapping of lightning discharge processes, *J. Geophys. Res.*, *83* (C7), 3575-3583, 1978.

Taylor, W.L., E.A. Brandes, W.D. Rust, and D.R. MacGorman, Lightning activity and severe storm structure, *Geophys. Res. Lett.*, *11* (5), 545-548, 1984.

Tierney, H.i., A.R. Jacobson, W.H. Beasley, and P.E. Argo, Determination of source thunderstorms for VHF emissions observed by the FORTE satellite, *Radio Sci.*, *36* (1), 79, 2001.

Willett, J.C., J.C. Bailey, C. Leteinturier, and E.P. Krider, Lightning electromagnetic radiation field spectra in the interval from 0.2 to 20 MHz, *J. Geophys. Res.*, *95* (D12), 20,367-20,387, 1990.

Willett, J.C., E.P. Krider, and C. Leteinturier, Submicrosecond field variations during the onset of first return strokes in cloud-to-ground lightning, *J. Geophys. Res.*, *103* (D8), 9027-9034, 1998.

Zipser, E.J., Deep cumulonimbus cloud systems in the tropics with and without lightning, *Mon. Weather Rev.*, *122* (8), 1837-1851, 1994.

Zipser, E.J., and K.R. Lutz, The vertical profile of radar reflectivity of convective cells: A strong indicator of storm intensity and lightning probability?, *Mon. Weath. Rev.*, *122* (8), 1751-1759, 1994.

Acknowledgements

The work described here was performed under the auspices of the United States Department of Energy. We are indebted to the FORTE operations team, led by Phil Klingner and Diane Roussel-Dupré, for constant support in acquiring and working with FORTE data. We are also indebted to Drs. Kenneth Cummins, Martin Murphy, Paul Krehbiel, Hugh Christian, Anne Bondiou-Clergerie, John Willett, and Earle Williams for useful discussions and insights.

Table 1: Contemporaneous background and closely coincident NLDN strokes

land strokes	**-CG**	**+CG**	**IC**
contemporaneous NLDN background	1,200,554	96,407	13,954
NLDN strokes closely coincident with FORTE events	5,097	3,941	1,237
ratio of closely coincident to background	**0.004**	**0.041**	**0.089**
sea strokes	**-CG**	**+CG**	**IC**
contemporaneous NLDN background	251,026	10,650	1,514
NLDN strokes closely coincident with FORTE events	4,816	976	420
ratio of closely coincident to background	**0.019**	**0.092**	**0.277**

Table 2: Contemporaneous background and closely coincident NLDN strokes for the two specific storms in Section 4

continental storm	**-CG**	**+CG**	**IC**
contemporaneous NLDN background	1,995	113	23
NLDN strokes closely coincident with FORTE events	24	8	12
ratio of closely coincident to background	**0.012**	**0.070**	**0.52**
marine storm	**-CG**	**+CG**	**IC**
contemporaneous NLDN background	271	4	0
NLDN strokes closely coincident with FORTE events	2	3	0
ratio of closely coincident to background	**0.007**	**0.75**	**_____**